Structural properties of thermoresponsive poly(*N*-isopropylacrylamide)-poly(ethyleneglycol) microgels

J. Clara-Rahola,[1,2,a)] A. Fernandez-Nieves,[2,b)] B. Sierra-Martin,[1,c)] A. B. South,[3,d)] L. A. Lyon,[3,e)] J. Kohlbrecher,[4,f)] and A. Fernandez Barbero[1,g)]
[1]*Group of Complex Fluids, Applied Physics Department, University of Almeria, Almeria ES-04120, Spain*
[2]*School of Physics, Georgia Institute of Technology, Atlanta, Georgia 30332, USA*
[3]*School of Chemistry and Biochemistry and Petit Institute for Bioengineering & Bioscience, Georgia Institute of Technology, Atlanta, Georgia 30332, USA*
[4]*Laboratory for Neutron Scattering, Paul Scherrer Institut, CH-5232 Villigen, Switzerland*

(Received 13 February 2012; accepted 15 May 2012; published online 7 June 2012)

We present investigations of the structural properties of thermoresponsive poly(*N*-isopropylacrylamide) (PNiPAM) microgels dispersed in an aqueous solvent. In this particular work poly(ethyleneglycol) (PEG) units flanked with acrylate groups are employed as cross-linkers, providing an architecture designed to resist protein fouling. Dynamic light scattering (DLS), static light scattering (SLS), and small angle neutron scattering (SANS) are employed to study the microgels as a function of temperature over the range $10\,^{\circ}\mathrm{C} \leq T \leq 40\,^{\circ}\mathrm{C}$. DLS and SLS measurements are simultaneously performed and, respectively, allow determination of the particle hydrodynamic radius, R_h, and radius of gyration, R_g, at each temperature. The thermal variation of these magnitudes reveals the microgel deswelling at the PNiPAM lower critical solution temperature (LCST). However, the hydrodynamic radius displays a second transition to larger radii at temperatures $T \leq 20\,^{\circ}\mathrm{C}$. This feature is atypical in standard PNiPAM microgels and suggests a structural reconfiguration within the polymer network at those temperatures. To better understand this behavior we perform neutron scattering measurements at different temperatures. In striking contrast to the scattering profile of soft sphere microgels, the SANS profiles for $T \leq$ LCST of our PNiPAM-PEG suspensions indicate that the particles exhibit structural properties characteristic of star polymer configurations. The star polymer radius of gyration and correlation length gradually decrease with increasing temperature despite maintenance of the star polymer configuration. At temperatures above the LCST, the scattered SANS intensity is typical of soft sphere systems. © *2012 American Institute of Physics*. [http://dx.doi.org/10.1063/1.4723686]

I. INTRODUCTION

Microgel particle suspensions have attracted increasing interest in the field of soft condensed matter since their ability to swell or expand after a change in variables such as temperature, pH, or ionic strength allows the study of a broad range of phase behaviors within a single sample; this in addition allows for a wide variety of industrial applications.[1–4] Furthermore, due to their intra-particle structure and uneven or discontinuous mass distribution, microgel particles can deform and interpenetrate resulting in many cases in a strikingly different behavior compared to hard sphere suspensions.[5–7] In this work we aim to study the structure of thermally responsive poly(*N*-isopropylacrylamide) microgels cross-linked with poly(ethylene glycol diacrylate) (PNiPAM-PEG) at different temperatures by employing a variety of scattering techniques. This particular system is a relatively new class of microgel particle wherein PEG is employed as cross-linker of the linear PNiPAM.[8] PEG is a hydrophilic non-degradable polymer extensively used in biotechnology, as it is biocompatible, non-toxic, non-immunogenic, and soluble in water. Moreover, studies of these PEG cross-linked microgels have illustrated their utility in biotechnological applications[9–12] as PEG facilitates control of protein adsorption and minimizes non-specific cell adhesion.[13,14] Thus, PNiPAM-PEG microgels represent a promising system that can be employed not only in fundamental research but also in bio- and nano-technological applications such as controlled drug delivery.[15]

We study the morphology of this class of microgel system by employing static and dynamic light scattering (SLS and DLS, respectively) as well as small angle neutron scattering (SANS). A double volume transition induced by temperature is observed, the first one at 17 °C and the second one at 32 °C, which corresponds to the lower critical solution temperature (LCST) of PNiPAM. These transitions determine three temperature ranges where microgels display distinct structural features which we describe through a combination of soft particle and star-polymer models. The nature of both transitions is discussed by proposing as mechanisms, the standard transition associated to PNiPAM solubility at the LCST, and a

a)Author to whom correspondence should be addressed. Electronic addresses: joaquim.clara-rahola@physics.gatech.edu and quimtxo@ual.es.
b)Electronic mail: alberto.fernandez@physics.gatech.edu.
c)Electronic mail: bsierra@ual.es.
d)Electronic mail: bonhivac@gmail.com.
e)Electronic mail: lyon@gatech.edu.
f)Electronic mail: joachim.kohlbrecher@psi.ch.
g)Electronic mail: afernand@ual.es.

desolvation transition due to the heterogeneous distribution of PEG segments into the particles at 17 °C.

II. PARTICLE SYNTHESIS

A. Materials

All reagents are purchased from Sigma-Aldrich unless otherwise specified. The monomer *N*-isopropylacrylamide (NiPAM) is recrystallized from hexanes (J.T. Baker) and dried under vacuum prior to use. The cross-linker poly(ethylene glycol) diacrylate with average Mw = 700 (PEG-diacrylate), surfactant sodium dodecyl sulfate (SDS), and initiator ammonium persulfate (APS) are used as received. Water used throughout the synthesis is house distilled and deionized to a resistance of at least 18 MΩ (Barnstead Thermolyne E-Pure system).

B. Microgel synthesis

Microgels are synthesized by aqueous free radical precipitation polymerization using a total monomer concentration of 70 mM and total volume of 1 L. The molar composition consists of 98% NiPAM (7.76 g) and 2% PEG-diacrylate (1.03 mL). Surfactant SDS is used at a concentration of 1 mM (0.2884 g). The aqueous monomer and surfactant solution is stirred in a 2 L three-neck round bottom flask and purged with N_2 for approximately 1 h while the solution is heated to 70 °C. The initiator ammonium persulfate (0.2282 g) is dissolved in 1 mL of deionized water and added to initiate the polymerization (1 mM final concentration). The reaction is allowed to proceed for 4 h at 70 °C under a blanket of N_2. Microgels of this composition have been shown previously to resist aggregation and non-specific protein adsorption at temperatures above the PNiPAM LCST.[8–12] The inferred hydrophilicity of the particles at elevated temperatures has been ascribed to surface-segregation of PEG segments; this has been confirmed by variable temperature ^{1}H NMR measurements.[8] Once the microgels are obtained, the system is lyophilized and further redispersed in D_2O at a concentration $c = 1$ mg/mL.

III. RESULTS AND DISCUSSION

A. SLS and DLS on PNiPAM-PEG microgels

DLS and SLS are performed on dilute D_2O suspensions of PNiPAM-PEG particles in order to monitor microgel size variation with temperature. We employ a Malvern 4700 multiangle scattering instrument that allows measuring the already volume corrected static scattering properties of our microgels. The accessible q-range of this instrument allows resolving the Guinier regime of our PNiPAM-PEG microgels as illustrated in Figure 1(a). In this regime, the SLS intensity is hallmarked by decaying exponentially, $I(q) \sim \exp[-q^2 R_g^{2/3}]$, with R_g the radius of gyration at each temperature.[16] The exponential decay of the SLS form factors gradually rises with increasing temperature and the scattered intensity at low q rises as well. This suggests microgel deswelling with increasing temperature: smaller particles displace their form factor minima to larger q, while concomitantly the microgel-solvent optical contrast increases as solvent is expelled with particle shrinking. The Malvern 4700 multiangle scattering unit allows performance of DLS experiments simultaneously with SLS measurements where the intensity correlation function, $g_I(\tau)$, is recorded. As our samples are ergodic, we relate the intensity correlation function to the field correlation function, $g_E(\tau)$, through the Siegert relation: $g_I(\tau) - 1 = \beta[g_E(\tau)]^2$, where τ is the correlation lag-time and β is the coherent factor.[17] Consistent with SLS results, the decay time of $g_E(\tau)$ decreases with increasing temperature, as illustrated in Figure 1(b) where the temperature evolution of the experimental $(g_I(\tau) - 1)/\beta$ is shown. This also indicates microgel deswelling, as smaller particles diffuse faster than larger particles causing light de-correlation at shorter times. The correlation function is well described by $(g_I(\tau) - 1)/\beta = [g_E(\tau)]^2 \sim \exp[-2q^2 D\tau]$, with D the diffusion coefficient and q the scattering vector.[17] The hydrodynamic radius, R_h, is inversely proportional to D through the Stokes-Einstein relation, $D = k_B T/6\pi\eta R_h$, with η the solvent viscosity, T the system temperature, and k_B the Boltzmann constant; it is thus straightforward to quantify how the hydrodynamic radius depends on temperature from our DLS measurements.

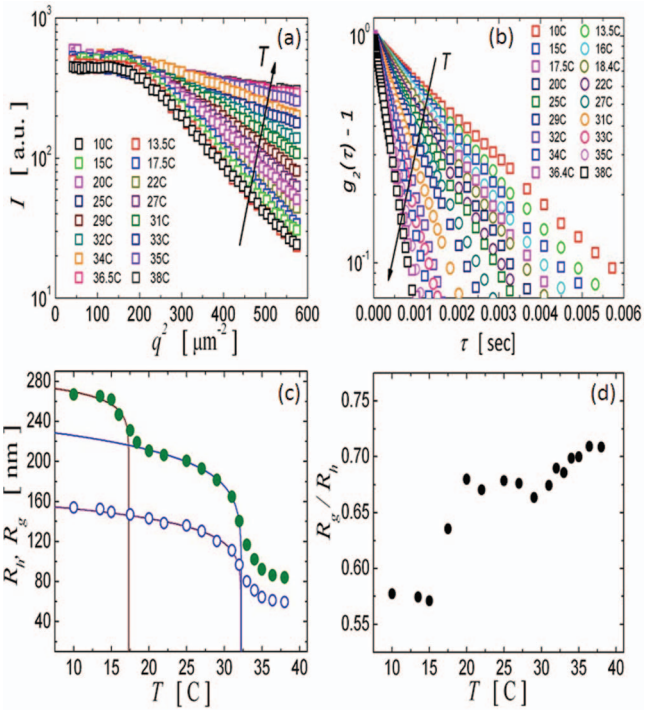

FIG. 1. SLS intensity profiles (a) and normalized DLS intensity correlation functions (b) of diluted PNiPAM-PEG microgel systems at different temperatures. The temperature evolution (c) of R_h (filled symbols) and R_g (open symbols) reveals an initial transition for R_h at low temperatures besides the one at the PNiPAM LCST. The solid lines are fits according to the functional form $R = R_0(T_t - T)^\alpha$. The ratio R_g/R_h denotes the particle softness and hardness at different temperature ranges (d).

An unusual behavior is found when the SLS radii of gyration and the DLS hydrodynamic radii are correlated with temperature. The static radius of gyration, R_g, gradually decreases with increasing temperature and exhibits a swift

TABLE I. Fitting parameters for R_h (DLS) and R_g (SLS) to the functional form $R(T) = R_0\ (T_t - T)^{\alpha}$ (right panel). Fitting parameters for the excluded volume screening-length ξ (SANS) to $\xi(T) = \xi_0\ (T_c - T)^{\varepsilon}$ (left panel).

	Light scattering			Neutron scattering		
	R_0 (nm)	T_t (°C)	α	ξ_0 (nm)	T_c (°C)	ε
Low-temperature transition						
DLS	248	17.30	0.0413	34	19.10	0.0742
High-temperature transition						
DLS	160	32.25	0.1125	21	32.35	0.1272
SLS	108	32.20	0.1105			

reduction to a minimum size at the PNiPAM LCST, as shown in Figure 1(c). Here it is verified that at the q-window where the SLS form factors decay exponentially, $qR_g \sim 1$, which further emphasizes that the Guinier region is resolved. However and in striking contrast to the temperature evolution of R_g, the magnitude of R_h decays to an intermediate plateau and gradually decreases until the LCST is attained. At the LCST and at higher temperatures the hydrodynamic radius collapses down to a minimum length due to poor PNiPAM hydration, as shown in Figure 1(c). The two temperature transitions of R_h and the single temperature transition of R_g are well described by a critical-like functional form, $R \sim R_0\ [T_t - T]^{\alpha}$, where α is a critical exponent and R_0 is the particle radius at a temperature much lower than the transition temperature, T_t. The magnitude of these fitting parameters is presented in Table I. Note that the T_t corresponding to the LCST for both R_g and R_h agree with each other and that the critical exponent α is also remarkably close in both cases. Note as well that the hydrodynamic radii are significantly larger than the radii of gyration. This can be attributed to an uneven mass distribution inside the particle: the mass density is larger in the central part of the microgel compared to its periphery, suggesting a core-shell-like structure of the particle. Within this scope the asymmetrical mass distribution in the particle becomes more balanced at higher temperatures and in particular above the LCST.

We also explore the temperature variation of the R_g/R_h ratio which is typically found to be $R_g/R_h = 0.775$ for hard sphere systems and $R_g/R_h = 0.61$ for soft sphere systems[16,18] and plot the results in Figure 1(d). Above the PNiPAM LCST we obtain $R_g/R_h \sim 0.71$, which indicates that even at these high temperatures the particles are less dense at their periphery, a result that can be explained considering PEG segregation towards the surface at these temperatures.[8] Below the LCST, $R_g/R_h \sim 0.67$ further emphasizing that in our microgel system the polymer density decreases from the center towards the periphery of the particle. For even lower temperatures, $T \leq 17.3\,^{\circ}$C, below the initial temperature-transition of R_h, $R_g/R_h = 0.57$. These results further suggest a core-shell structure for these microgels, with a varying contribution of each part depending on the temperature. Below 17 °C, PEG and PNiPAM chains are fully swollen, while above this temperature and below the LCST, PNiPAM-PNiPAM interactions start to appear, as indicated by previous spectroscopy studies of PNiPAM-PEG block-copolymers, which suggest that the contraction of the PNiPAM block starts to occur at 17–18 °C.[19] However, these interactions are not dominant over solvent-PNiPAM interactions in this temperature range. A massive predominant core is still present and it is responsible for the static properties described by R_g. Therefore, in the low temperature range, there is a particle shell that is fully swollen and that we deem responsible for the low temperature increase of R_h. At intermediate temperatures and due to a more favorable hydration, PEG is predominant at the outer regions of our particles while PNiPAM located in the shell starts to collapse. Here the outer PEG density is rather low and provides poor contrast when compared with the static scattering of the overall particle and is thus not seen in SLS. Above the LCST, PNiPAM chains collapse resulting in the particle shrinkage to a minimal size, while PEG remains predominantly at the microgel surface.

B. Small angle neutron scattering on PNIPAM-PEG microgels

SANS experiments are performed in the SANS-1 line of the Paul Scherrer Institut[20] (PSI), Switzerland, with the aim to better understand the behavior of our PNiPAM-PEG microgels. Using an incident mean neutron wavelength of $\lambda = 0.6$ nm with a wavelength broadening of $\Delta\lambda/\lambda = 10\%$ (FWHM) and 3 detector position we could cover a q-range between $2.5\ \mu\text{m}^{-1} < q < 350\ \mu\text{m}^{-1}$. The data were corrected in the usual way for background scattering, detector efficiency, and solid-angle distortion and normalized to absolute units by means of a solvent sample using the BerSANS software package.[21]

As in DLS and SLS experiments we span a temperature range $10\,^{\circ}\text{C} \leq T \leq 45\,^{\circ}\text{C}$. At temperatures, $T \leq 17\,^{\circ}$C, the neutron scattered intensity drops sharply at low q and progressively decreases for $q > 60\ \mu\text{m}^{-1}$, as shown in Figure 2(a) for $T = 10\,^{\circ}$C. At higher T, the neutron intensity profile is displaced to higher q. However, when the temperature is close, yet still below the LCST, a feature reminiscent of an inflection point appears, as shown also in Figure 2(a) for $T = 32\,^{\circ}$C. Once the LCST is crossed, the SANS intensity exhibits two distinct inflection points, followed by a q^{-4} intensity decay, as shown in Figure 2(b) for $T = 40\,^{\circ}$C.

1. Star polymer approach

The SANS profiles at low temperatures are highly reminiscent of core-shell form factors,[22–24] which is indeed the nature of our microgels. However, classic core-shell soft sphere models do not satisfactorily describe the rich behavior observed in our data. For low T, $R_g/R_h \sim 0.57$, which indicates the extremely open core-shell structure of the particles in this temperature range. Indeed, a R_g/R_h ratio below 0.61 indicates an open structure down to a length scale set by the radius of a small massive core, which we identify with R_g. As a result, we use a star polymer form factor to describe the SANS data

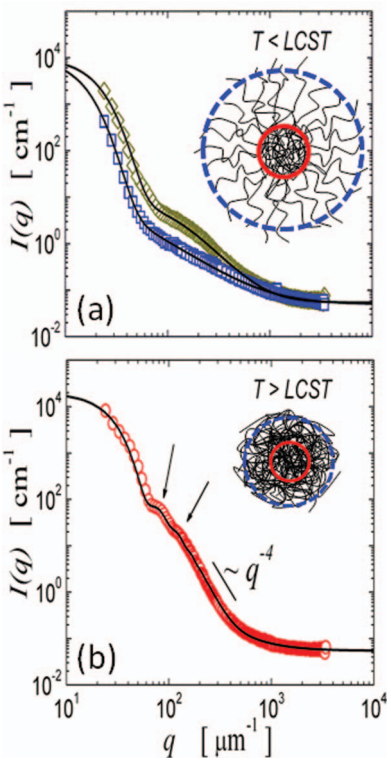

FIG. 2. SANS intensity profiles of PNIPAM-PEG suspensions at (a) T = 10 °C (blue squares), T = 32 °C (yellow diamonds), and (b) T = 40 °C (red circles). The black lines are the fits according to (a) the star polymer described by Eq. (1) and (b) the soft sphere models described by Eq. (2).

at low temperatures:[25,26]

$$P_{starpolym}(q) = A_1 \int \rho\left(R_g^N, \delta\right) \exp\left(-q^2 R_g^{N^2}/3\right) dR_g^N + \frac{A_2}{q\xi} \frac{\sin(\mu \tan^{-1}(q\xi))}{(1+q^2\xi^2)^{\mu/2}} + I_0 \quad (1)$$

where $\mu = 1/\nu - 1$, with ν the Flory solvency parameter, and ξ the polymer excluded volume correlation length inside the star.[27] The first term in Eq. (1) describes the first decay of the SANS profiles; it corresponds to a Guinier approximation and provides the microgel SANS radius of gyration, R_g^N. We further consider that R_g^N is polydisperse according to a Gaussian distribution, $\rho(R_g^N, \delta)$, of width δ. Due to the internal structure of our particles, the second term describes the inner part of the microgel through a blob structure of size ξ. It is quantitatively described by the Fourier transform of the mass density correlation function inside the star and accounts for the polymer structure within the shell of the microgel particle. The weight of each contribution is provided by the corresponding amplitudes, A_1 and A_2.[28] We fit the experimental data using Eq. (1) and minimizing $\chi^2 = [P(q) - P_{starpolym}(q)]^2$, leaving A_1, A_2, R_g^N, δ, ξ, and μ as free parameters; $P(q)$ is our experimental form factor. The magnitude I_0 in Eq. (1) simply accounts for the incoherent scattering of the sample. Figure 2(a) shows the excellent agreement between the star-polymer prediction and the experimental form factor at $T = 10$ °C. The agreement is also found at $T = 13.5$ °C and $T = 15$ °C, at higher temperatures and even at $T = 32$ °C, as shown in Figure 2(a).[28]

2. Soft sphere approach

The star polymer form factor no longer describes our SANS data for temperatures above the PNiPAM LCST. Instead, we use a model originally proposed for micelles which effectively describes the structural features of other microgel systems. In this model the spherical particle is depicted with a fuzzy surface and characterized by an inhomogeneous mass distribution through the microgel.[29,30] Microgels whose structure is well described by this model typically exhibit $0.61 < R_g/R_h < 0.775$, emphasizing their soft character. The form factor is described by the following functional form:

$$P_{soft\,sphere}(q) = A_3 \int \rho(R,\gamma) \left[\frac{3}{(qR)^3} [\sin(qR) - qR\cos(qR)] \exp\left[-\frac{(\sigma q)^2}{2}\right] \right]^2 dR + \frac{A_4}{1+(q\zeta)^2} + I_0 \quad (2)$$

Here σ represents the extent of the fuzzy surface around the micogel and R is the core radius. We consider polydispersity in R according to a Gaussian distribution, $\rho(R, \gamma)$, with γ the width of the distribution. The first term dominates at low q-values and describes the overall microgel particle as a sphere with a fuzzy surface. The second term dominates at larger q and describes the microgel structure at length scales below the size of the overall particle. This contribution is thus related to the characteristic mesh size of the network, ζ. We fit our data by minimizing $\chi^2 = [P(q) - P_{soft\ sphere}(q)]^2$ with R, γ, σ, and ζ as fitting parameters. Also, seemingly to the model at temperatures below the LCST, A_3 and A_4 are fitting amplitudes.[28] Note that as in Eq. (1), I_0 is again a constant to be added in order to describe the incoherent scattering from the sample. This model correctly describes the experimental data, as shown in Figure 2(b) for $T = 40$ °C. We correctly capture the presence of the two inflection points, which are features reminiscent of the core contribution to the form factor in this q-range, and the decay at larger q reflecting the internal structure of the particle.[28]

3. Structural information

The double description proposed in this work separates the PNiPAM-PEG configuration into two distinct regimes. Below the LCST, particles are characterized by a low density open structure and hence a structure that strikingly resembles a star polymer. In this regime, the excluded volume correlation length, ξ, has a temperature response remarkably similar to the one exhibited by the hydrodynamic radius and can be described using the same critical-like expressions that successfully described the two steps in R_h: $\xi = \xi_0(T_c - T)^{\varepsilon}$, with T_c a critical temperature and ε a critical exponent. The fits of the data to this functional form are shown in

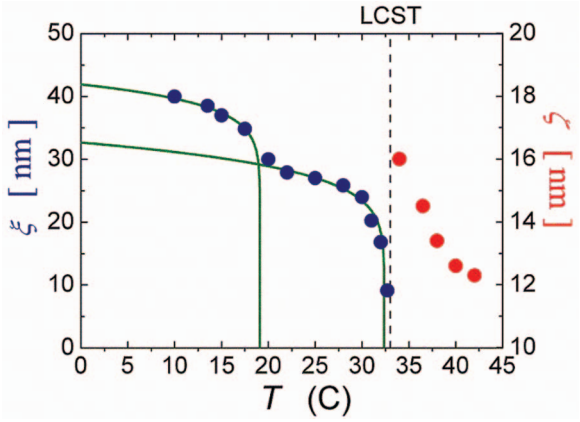

FIG. 3. Temperature evolution of the excluded volume screening length ξ (blue symbols) and network correlation length ζ (red symbols). The green lines are fits of the ξ temperature transitions to a critical power law $\xi = \xi_0 (T_c - T)^{\varepsilon}$. The vertical dotted line indicates the position of the PNiPAM LCST.

Figure 3 and the magnitude of each fitting parameter is displayed in Table I. Both T_c and ε are in remarkable agreement with the results obtained from the fits of R_h, reflecting the affine shrinkage of the particles in this temperature range. In contrast to this behavior, the radius of gyration determined by SANS, R_g^N, only displays a single transition at the LCST as described in Figure 4, consistent with the behavior obtained by light scattering and further supporting our previous interpretation that our PNiPAM-PEG microgels can be treated as having a dense core surrounded by a significantly lower density shell for temperatures below the LCST. Additionally, for $T \leq 17\,^{\circ}$C the shell behavior seems decoupled from the behavior of the core: ξ increases with decreasing temperature, while R_g is essentially temperature independent.

For temperatures above the LCST, our PNiPAM-PEG microgels are best described as soft spheres. In this temperature range, the network mesh size, ζ, exhibits an asymptotic behavior when the temperature is close to the LCST; ζ decreases

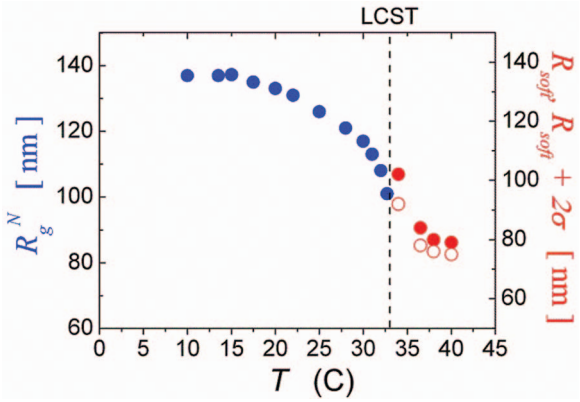

FIG. 4. Blue symbols are the radii of gyration, R_g^N, resolved from SANS profiles fitted to the star polymer approximation (Eq. (1)). Red open symbols are the microgel radii and red closed symbols are the fuzzy soft sphere lengths added to the soft sphere radii, both resolved from SANS profiles fitted to the soft sphere approximation (Eq. (2)). The dotted vertical line denotes the PNiPAM LCST.

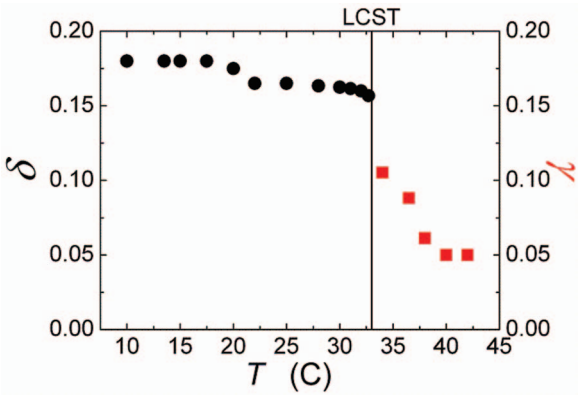

FIG. 5. Polydispersity indexes of PNiPAM-PEG microgels at temperatures below and above the LCST.

with increasing temperature, as shown in Figure 3. Such behavior is usually found for other soft particles.[30] Therefore, at temperatures above the LCST the core-shell configuration is most compact, with a dense core and a dense shell. Moreover, note that the soft sphere radius plus the fuzzy surface width, $R + 2\sigma$, obtained from the fits of the data to the microgel model described by Eq. (2) and shown in Figure 4 is in agreement with the hydrodynamic radius shown in Figure 1, consistent with what has been found for microgels.[29] It is worthwhile mentioning that the polydispersity index δ is rather high at low temperatures; as observed in Figure 5. In the 10–17 °C range it reaches a magnitude 0.18 and interestingly it slightly decreases to a plateau at around 17 °C until the LCST is approached, where δ further decreases. This feature reminds the temperature behavior of the hydrodynamic radius R_h and the volume correlation length ξ and suggests that microgel deswelling with increasing temperature is homogeneous throughout the sample. Observe as well in Figure 5 that when the LCST is crossed the polydispersity index γ reaches a minimum magnitude of 0.05 indicating that a reasonably monodisperse system is achieved. Moreover, the magnitude and response of the sample polydispersity with temperature concurs with the proposed scenario as the low temperature open star polymer structure allows for a higher extent in polydispersity than the smaller and more compact high temperature soft sphere configuration.

In the low temperature region, we obtain a constant Flory exponent of $\nu = 0.95$ as shown in Figure 6. This constancy

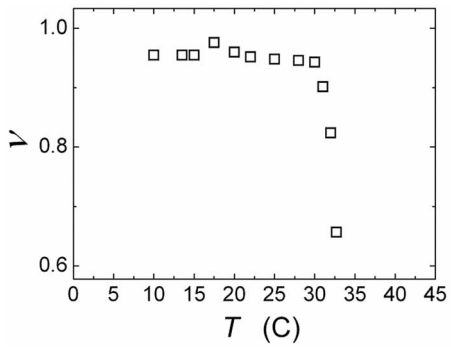

FIG. 6. Temperature evolution of the Flory parameter ν at temperatures below the PNiPAM LCST.

remains up to $T \sim 30\,^{\circ}$C. Beyond this point, ν drops to $\sim$0.6. In dilute solution, this exponent controls the overall size of a polymer chain. Magnitudes of $\nu = 1/2$ and $\nu = 3/5$ are expected for random walk and self-avoiding polymers, respectively, while $\nu = 1$ reflects a fully stretched polymer chain.[31] The evolution of ν thus reflects the evolution of our chains from a stretched situation, consistent with a swollen star polymer morphology, to a self-avoiding walk configuration on the approach to the LCST. The observed decrease in ν thus anticipates the observed deviation of the SANS data from a star polymer model on the approach to the soft sphere model that correctly describes our data for $T >$ LCST.

We emphasize that while the structure of our PNiPAM-PEG microgels, which contains segments composed of PNiPAM cross-linked with short PEG segments, is certainly different from the widely investigated block-copolymer-PNiPAM structures,[6,30,32,33] the low temperature transition we observe could result from the phase behavior observed in this other system.[19] In the block-copolymer structure at temperatures above 17 °C, PEG-PNiPAM micelles began showing a hydrophilic-to-hydrophobic transition, as evidenced by pyrene partitioning and spectroscopic signatures. This transition was also evident in the phase diagram for the polymers. These results were interpreted as a selective solvation effect where PNiPAM segments that were in PEG-rich regions were selectively desolvated by the PEG, leading to local phase separation of those PNiPAM segments. In our present system, a similar phenomenon would lead to surface localization of the PEG-rich segments and hence a very diffuse microgel structure. The decrease in R_h at 17 °C is therefore likely associated with a small amount of surface (PNiPAM-based) collapse during the PEG-PNiPAM phase separation. We note that since the majority of the particle mass is still core-localized, this transition is not observed in R_g.

IV. CONCLUSIONS

We study the structure of PNiPAM-PEG microgel particles in D_2O where PEG is employed as cross-linker. This system exhibits a striking double size transition, in contrast to the single transition found in typical PNiPAM-based microgels. Different scattering techniques evidence an initial transition at low temperatures, $T = 17\,^{\circ}$C, in addition to the particle collapse at the PNiPAM LCST. Correlation functions from DLS experiments allow the determination of the hydrodynamic radius, R_h, for which this double size transition is well observed. We also measure the structural radius of gyration, R_g, using SLS and SANS experiments. In contrast to the behavior of R_h, R_g only exhibits the LCST transition. Moreover, the magnitude of R_g is significantly smaller than R_h suggesting a core-shell particle structure with a larger mass density in the core than in the shell. In addition, SANS measurements below the PNiPAM LCST display microgel form factors that can be described by a star polymer model, supporting the scenario of a core-shell mass density profile within the particle. The structural polymer excluded volume length exhibits a double transition as well. Above the LCST the system achieves its minimal size and has a dense core and a dense shell. As a result, in this temperature range, the microgel form factor is well described by a soft sphere model.

ACKNOWLEDGMENTS

The authors thank financial support from the Spanish Science and Innovation Ministry (grant MAT2011-28385), the Andalucian Government (Projects: P010-FQM 06104 and P07-FQM-03116), FEDER program, EU funded NMI3 program and from the COST Action-CM1101. Funding from the American NSF through GaTech MRSEC (DMR-0820382) and from the ACS Petroleum Research Fund (PRF 50603-DNI7) are also greatly appreciated. We also wish to thank Dr. Rafael Contreras Cáceres for fruitful discussions.

[1] G. Romeo, A. Fernandez-Nieves, H. W. Hyss, D. Acierno, and D. A. Weitz, Adv. Mater. **22**, 3441 (2010).
[2] J. Mattsson, H. M. Wyss, A. Fernandez-Nieves, K. Miyazaki, Z. Hu, D. R. Reichman, and D. A. Weitz, Nature (London) **462**, 83 (2009).
[3] R. Contreras-Cáceres, J. Pacifico, I. Pastoriza-Santos, J. Pérez-Juste, A. Fernández-Barbero, and L. M. Liz-Marzan, Adv. Funct. Mater. **19**, 1 (2009).
[4] A. Fernandez-Nieves, A. Fernandez-Barbero, B. Vincent, and F. J. de las Nieves, Langmuir **17**, 1841 (2001).
[5] B. H. Tan, K. C. Tam, Y. C. Lam, and C. B. Tan, Langmuir **21**, 4283 (2005).
[6] M. Stieger, J. S. Pedersen, P. Linder, and W. Richtering, Langmuir **20**, 7283 (2004).
[7] J. J. Lietor-Santos, C. Kim, M. L. Lynch, A. Fernandez-Nieves, and D. A. Weitz, Langmuir **26**, 3174 (2010).
[8] Daoji Gan and L. Andrew Lyon, Macromolecules **35**, 9634 (2002).
[9] A. W. Bridges, N. Singh, K. L. Burns, J. E. Babensee, L. A. Lyon, and A. J. Garcia, Biomaterials **29**, 4605 (2008).
[10] A. W. Bridges, R. E. Whitmire, N. Singh, K. L. Templeman, J. E. Babensee, L. A. Lyon, and A. J. Garcia, J. Biomed. Mater. Res. A **94A**, 252 (2010).
[11] C. M. Nolan, C. D. Reyes, J. D. Debord, A. J. Garcia, and L. A. Lyon, Biomacromolecules **6**, 2032 (2005).
[12] N. Singh, A. W. Bridges, A. J. Garcia, and L. A. Lyon, Biomacromolecules **8**, 3271 (2007).
[13] A. Revzin, R. J. Russel, V. K. Yadavalli, W. G. Koh, C. Deister, D. D. Hile, M. B. Mellott, and M. Pishko, Langmuir **17**, 5440 (2001).
[14] E. Tziampazis, J. Kohn, and P. V. Moghe, Biomaterials **21**, 511 (2000).
[15] J. H. Ward and N. A. J. Peppas, J. Control. Rel. **71**, 183 (2001).
[16] P. N. Pusey, "Introduction to scattering experiments," in *Neutrons, X-Rays and Light: Scattering Methods Applied to Soft Condensed Matter*, edited by P. Linder and Th. Zemb (Elsevier, Amsterdam, 2002), p. 3.
[17] P. N. Pusey, "Dynamic light scattering," in *Neutrons, X-Rays and Light: Scattering Methods Applied to Soft Condensed Matter*, edited by P. Linder and Th. Zemb (Elsevier, Amsterdam, 2002), p. 203.
[18] A. Fernandez-Nieves, F. J. de las Nieves, and A. Fernandez-Barbero, J. Chem. Phys. **120**, 374 (2004).
[19] R. Motokawa, K. Morishita, S. Koizumi, T. Nakahira, and M. Annaka, Macromolecules **38**, 5748 (2005).
[20] J. Kohlbrecher and W. Wagner, J. Appl. Crystallogr. **33**, 804 (2000).
[21] U. Keiderling, Appl. Phys. A: Mater. Sci. Process. **74**, S1455 (2002).
[22] I. Berndt, J. S. Pedersen, and W. Richtering, Angew. Chem. **118**, 1769 (2006).
[23] T, Mason and M. Y. Lin, Phys. Rev. E **71**, 040801-1 (2005).
[24] I. Berndt, J. S. Pedersen, P. Linder, and W. Richtering, Langmuir **22**, 459 (2006).
[25] D. Richter, O. Jucknischke, L. Willner, L. J. Fetters, M. Lin, J. S. Huang, J. Roovers, C. Toporovski, and L. L. Zhou, J. Phys. IV **03**, C8-3 (1993).
[26] L. Willner, O. Jucknischke, D. Richter, J. Roovers, L.-L. Zhou, P. M. Toporowski, L. J. Fetters, J. S. Huang, M. Y. Lin, and N. Hadjichristidis, Macromolecules **27**, 3821 (1994).
[27] P. G. de Gennes, *Scaling Concepts in Polymer Physics* (Cornell University Press, NY, 1979).
[28] See supplementary material at http://dx.doi.org/10.1063/1.4723686 for the full SANS form factors at each sampled temperature with its corresponding model fit and also for a detailed description of the star polymer and soft sphere model fits along with the magnitude and temperature evolution of the weight amplitudes A_1, A_2, A_3, A_4.

[29]M. Stieger, W. Richtering, J. S. Pedersen, and P. Lindner, J. Chem. Phys. **120**, 6197 (2004).
[30]J. J. Lietor-Santos, U. Gasser, R. Vavrin, Z. B. Hu, and A. Fernandez-Nieves, Macromolecules **42**, 6225 (2009).
[31]P. J. Flory, *Principles of Polymer Chemistry* (Cornell University Press, 1983).
[32]T. Hu and C. Wu, Phys. Rev. Lett. **83**, 4105 (1999).
[33]T. Hu and C. Wu, Macromolecules **34**, 6802 (2001).